Progress In Electromagnetics Research C, Vol. 109, 275–287, 2021

A Triple-Band Antenna with a Metamaterial Slab for Gain Enhancement and Specific Absorption Rate (SAR) Reduction

Imaculate Rosaline*

Abstract—A compact triple-band antenna of size $20 \times 13 \times 1.6\,\text{mm}^3$ for WLAN (2.4/5 GHz) and WiMAX (3.5 GHz) applications and a metamaterial slab for Specific Absorption Rate (SAR) reduction are proposed in this paper. The antenna comprises a rectangular patch with two conjoint square split rings, attached along its top edge, to excite two resonances in the 2.5 GHz and 5.5 GHz range. The antenna is also backed with a slotted ground plane structure to achieve miniaturization. The radiator is subsequently slotted to yield the third tone around 3.5 GHz. Several parameters are tuned independently to achieve the desired bands of resonance around (2.2–2.6) GHz, (3.40–3.60) GHz, and (5.0–6.9) GHz with impedance bandwidths of 17%, 5.5%, and 46%, respectively. To validate the simulated results, the designed antenna is fabricated and measured experimentally. Later, a metamaterial slab composed of a 5×3 array of pentagonal split-rings printed on a $20 \times 13 \times 1.6\,\text{mm}^3$ FR-4 substrate is placed above the antenna at a suitable distance to increase the gain as well as to reduce the SAR. Inclusion of this slab improved the maximum radiation efficiency and gain of the proposed antenna from 65% and 2.7 dB to 80% and 3 dB. A cubical tissue model is designed and used for simulation. SAR reduction of 84.5% is inferred with the metamaterial slab. This paper has taken a cubical tissue model for SAR calculation, which can be further enhanced by taking a human phantom model in future.

1. INTRODUCTION

The limited availability of equipment space in modern smart devices demands the integration of several communication services onto a single device. Antenna being the heart of any communication device needs to be compact and simple while offering multiple operating bands. Microstrip antennas are always the best option to meet the aforesaid needs. The standard frequency allocations for WLAN and WiMAX applications designated by IEEE are (2.4–2.48) GHz — IEEE 802.11b/g, (3.4–3.69) GHz — IEEE 802.16e, and (5.15–5.35/5.75–5.825) GHz — IEEE 802.11a. Quite a lot of antennas are proposed in the literature for these applications. A defected ground plane structure [1, 2] is said to offer multiple bands by altering the current distribution along the feed line. Variably shaped radiators [3, 4] contribute to additional resonances and the frequency being dependent on their lengths and widths. An asymmetric coplanar strip fed monopole discussed in [5] offers compact size along with the desired bands of resonance. Radiating stubs and slots [6–8] offer additional band creation corresponding to their dimensions. Metamaterial based resonators and CRLH unit cells [9–12] are also employed in extra band conception by satisfying the properties of negative permeability or permittivity. The literature illustrates the design of several metamaterials and metasurfaces for antenna design for several applications like achieving wide bandwidth [13–16], miniaturization [17], travelling wave antenna [18], UHF-SHF band applications [19], and UWB wireless transceivers [20–22]. A flexible bow-tie antenna proposed in [23] is simple and easy to construct that is suitable for WLAN and WiMAX applications. However, many of these antennas suffer either complicated design or large size. Another important factor to be considered

Received 22 December 2020, Accepted 5 February 2021, Scheduled 16 February 2021
* Corresponding author: Imaculate Rosaline (rosaline@msrit.edu).
The author is with the Ramaiah Institute of Technology, Bangalore, India.

in the design of antennas is the Specific Absorption Rate (SAR), which should be maintained within the acceptable limits. According to International Commission on Non-Ionising Radiation Protection (ICNIRP) guidelines, the maximum acceptable SAR level on human body is 1.6 W/kg. An extensive literature survey on several techniques and materials for SAR reduction are discussed in [24, 25]. In recent years, electromagnetic metamaterials have been used widely for SAR reduction in the design of antennas [26–28]. A flexible dual-band antenna with a metamaterial structure for SAR reduction is shown in [29]. An embroidered metamaterial antenna based on an electromagnetic bandgap shielding structure is proposed in [30]. A metallic casing loop is proposed in [31] for SAR reduction. A multi split square ring metamaterial is proposed for SAR reduction in [32]. Many of these proposed metamaterials make use of negative permeability and permittivity characteristics in achieving reduction in the EM absorption.

This paper proposes a compact slotted rectangular antenna operating in the WLAN and WiMAX frequency ranges. The antenna comprises a slotted rectangular patch, two conjoint split rings, and a slotted ground plane. The conjoint split rings loaded on the radiator contribute to the dual-band behaviour, and a slot in the patch accounts for the third band of resonance. The slot in the ground plane is supportive in achieving size reduction of the proposed antenna. Subsequently, a metamaterial slab composed of a 5×3 array of pentagonal split rings is placed above the antenna at a suitable distance to increase gain as well as to reduce SAR.

The paper is organized as follows. The structure of the proposed antenna is presented in Section 2. Results are discussed in Section 3 highlighting a few parametric studies. Structure and analysis of the metamaterial slab are discussed in Section 4. Equivalent circuit model of the proposed antenna and the metamaterial slab are discussed in Section 5. SAR results with and without the metamaterial structure are highlighted in Section 6. The main conclusions are stated in Section 7.

2. STRUCTURE OF THE PROPOSED ANTENNA

The geometrical layout of the proposed slotted antenna with conjoint split rings is shown in Fig. 1. The antenna is printed on a $20 \times 13 \times 1.6\,\text{mm}^3$ FR-4 substrate ($\varepsilon_r = 4.4$ and $\tan\delta = 0.02$). The antenna is fed by a 3 mm wide 50 Ω microstrip line. The radiating structure is mainly composed of a slotted rectangular element and two conjoint split rings attached to it backed by a slotted ground plane. Photographs of the fabricated prototype are shown in Fig. 2. The design process involved in creating the

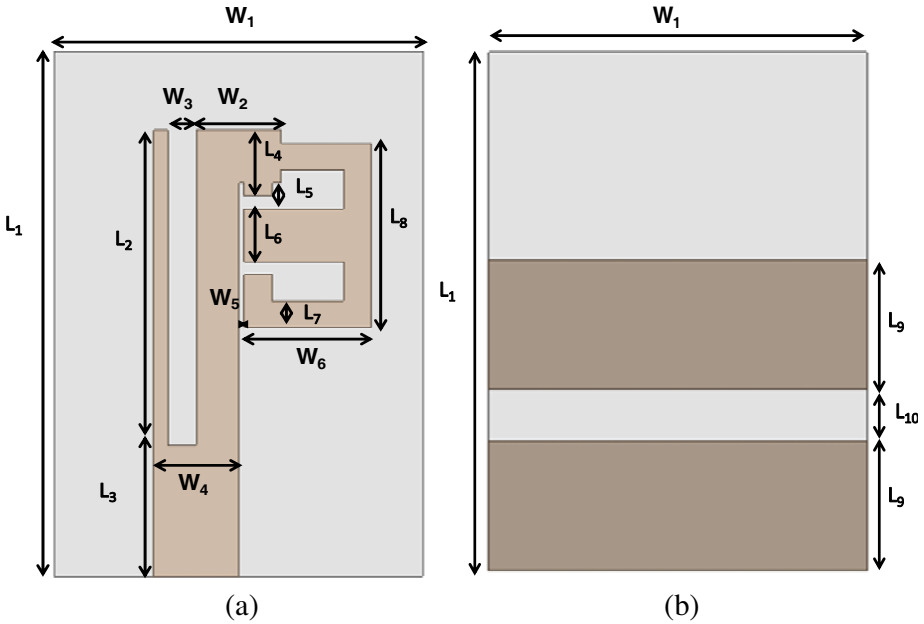

Figure 1. Geometrical layout of the proposed antenna. (a) Top view. (b) Bottom view.

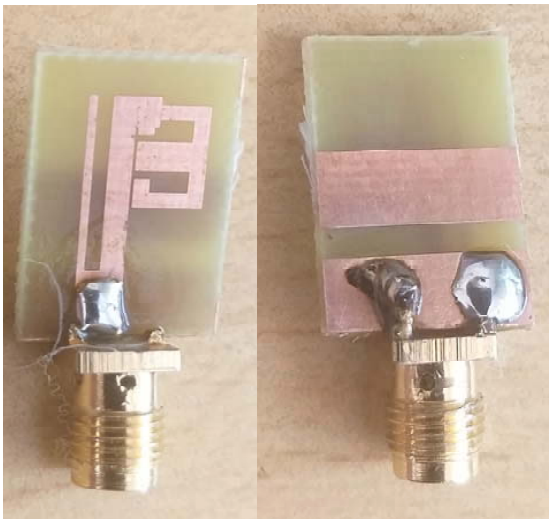

(a) (b)

Figure 2. Photograph of the proposed prototype. (a) Top view. (b) Bottom view.

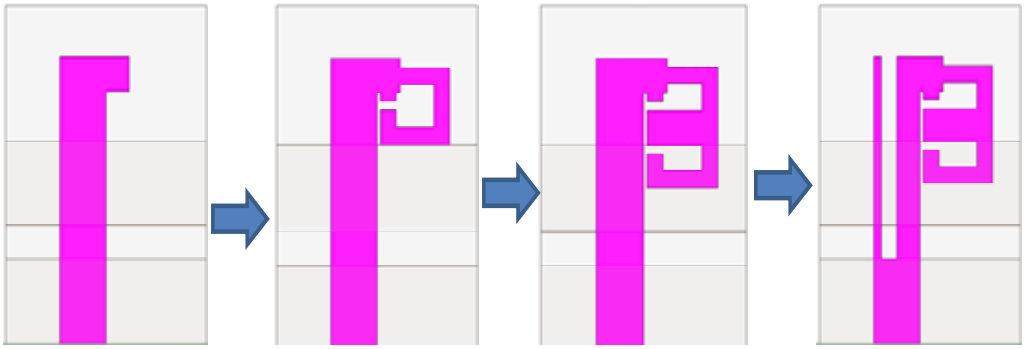

Figure 3. Evolution of the proposed antenna.

proposed structure is shown in Fig. 3. A comparison of the return loss characteristics of all the antennas involved in the design process is shown in Fig. 4. Antenna 1 shows an inverted L-shaped structure as the radiating element and a slotted ground plane at the bottom. This configuration exhibits a single resonant operating band at 4.2 GHz as shown in Fig. 4. The resonant frequency at 4.2 GHz is obtained by choosing the radiator length,

$$(L_2 + L_3) = \frac{\lambda}{2\sqrt{\varepsilon_r}} \cong 17\,\text{mm} \tag{1}$$

which approximately corresponds to half of the operating wavelength. In Antennas 2 and 3, two square split rings are loaded on the top edge of the radiator one after the other. Consequently, in Antenna 2, when the first split ring is loaded onto the L-shaped radiator, a new resonance is excited around 3 GHz. This resonance is due to the total length of the radiator and the split ring, $L_2+L_3+W_2/2+W_3+W_6 = 24\,\text{mm}$. This effective length corresponds approximately to half wavelength at 3 GHz, and the previously excited resonance is shifted to a higher frequency of 5.5 GHz. Loading one more split ring of same dimensions (Antenna 3) shifts the first resonance further, to a lower frequency value of 2.5 GHz due to the increased electrical path length, with a corresponding slight shift in the upper band (5 GHz). Subsequently, a slot is etched along the length of the main radiator (Antenna 4), whose perimeter ($2 \times L_2 + W_3 = 25\,\text{mm}$) also approximately corresponds to a half effective wavelength around 3.5 GHz, contributing to third resonant band and also improving the impedance matching at

Table 1. Parameters of the proposed antenna.

Parameter	Size (mm)	Parameter	Size (mm)
L_1	20	L_9	5
L_2	12	L_{10}	2
L_3	5	W_1	13
L_4	2.5	W_2	3
L_5	1	W_3	1
L_6	2	W_4	3
L_7	1	W_5	0.2
L_8	7	W_6	4.5

the higher resonant frequency (5 GHz). The parameters of the antenna are tuned variably to achieve the desired results. Table 1 lists the final dimensions of the proposed antenna.

3. RESULTS AND DISCUSSION

The return loss characteristics of the proposed antenna are simulated using Ansys High Frequency Structure Simulator V.19.1 and measured using a Vector Network Analyzer. As shown in Fig. 5, the simulated and measured results agree plausibly. The measured results show that the antenna resonance takes place at 2.35 GHz, 3.6 GHz, and 5.8 GHz with impedance bandwidths of 17%, 5.5%, and 46%. The measured results deviate from the simulated ones at upper resonant frequency, which is attributed to the fabrication intolerance and thick soldering of the SMA connector. However, the measured results have sufficient bandwidth to meet the requirements of WLAN and WiMAX applications. A few parameters in the antenna design are optimized to achieve frequency control. Fig. 6 shows the influence of width of the split ring (W_6) on the first band of resonance around 2.4 GHz. Antenna 3 is taken for this study. It is observed that as the width is increased, the antenna resonances are shifted towards lower frequency range. It is because the frequency and radiating element's length are inversely proportional. Thus, for our application, we have chosen $W_6 = 4.5$ mm, which corresponds to the fundamental tone around 3.1 GHz.

Next important parameter in the design of proposed antenna is the slot in the ground plane, which contributes to the size reduction of the antenna. The S_{11} (dB) plot is shown in Fig. 7 for slotted and un-slotted ground planes of Antenna 1. It is deduced that etching a rectangular slot on the ground

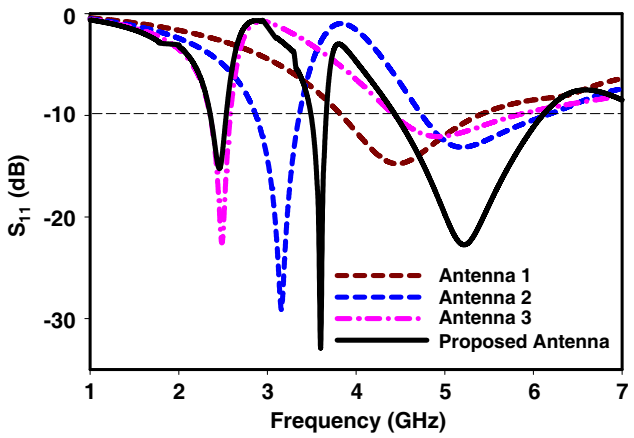

Figure 4. Simulated return loss characteristics of the antennas shown in Fig. 3.

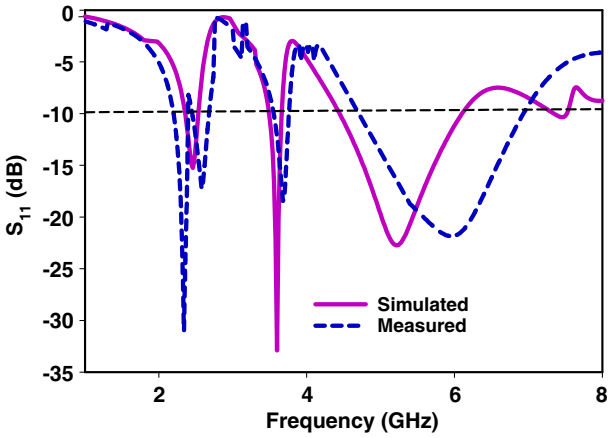

Figure 5. Simulated and measured return loss characteristics of the proposed antenna.

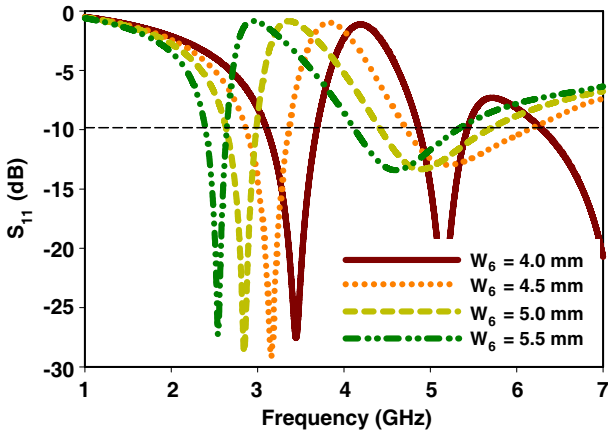

Figure 6. Return loss characteristics of the proposed antenna for various values of W_6.

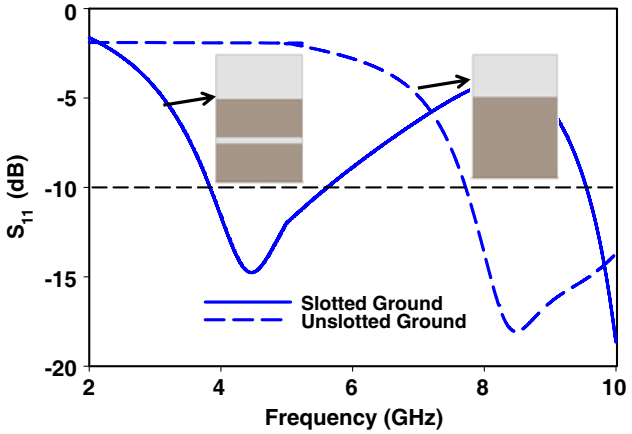

Figure 7. Simulated return loss characteristics of Antenna I with slotted and un-slotted ground plane.

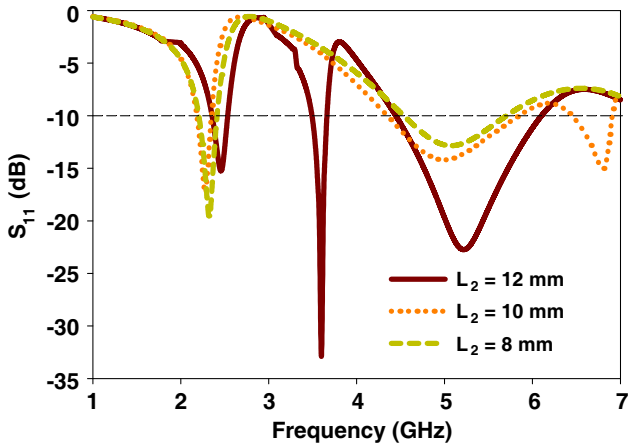

Figure 8. Return loss characteristics of the proposed antenna for various values of L_2.

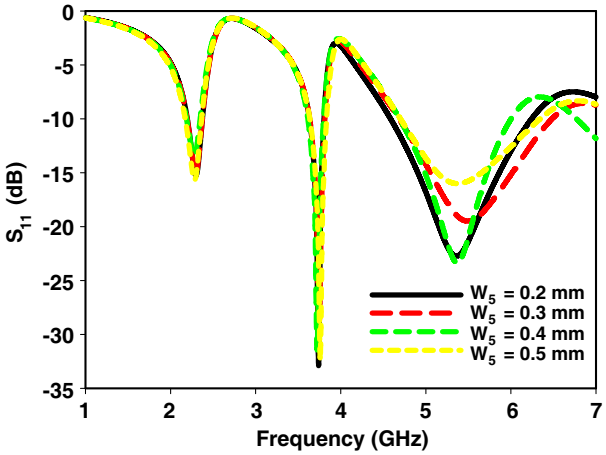

Figure 9. Return loss characteristics of the proposed antenna for various values of W_5.

plane increases the return current path length, thereby shifting the operating band from 8.4 GHz to 4.4 GHz, supporting miniaturization of the proposed antenna.

The conception of the middle band is dependent on the parameter L_2 as shown in Fig. 8. For smaller lengths up to 10 mm, only two WLAN bands are excited, but for a length of 12 mm, the slot width induces a capacitive effect, so a third band around 3.5 GHz is excited. The distance between the main radiator and conjoint split rings (W_5) is responsible for impedance matching around the 5 GHz resonant band. This is depicted in Fig. 9. As the distance is increased, impedance matching around 5 GHz is poor, and the bandwidth also decreases, while the other resonances remain unaltered. Hence, $W_5 = 0.2$ mm is chosen for our design, where a wide bandwidth and proper impedance matching are seen.

Simulated surface current distribution on the radiating element and the slotted ground plane at the centre frequencies of the three bands, 2.4 GHz, 3.5 GHz, and 5.5 GHz are shown in Fig. 10. It is observed that the current density is more along the width of the split ring at 2.4 GHz, along the length L_2 at 3.5 GHz, and along the length of the main radiator at 5.5 GHz. The current distribution on the upper portion of the ground plane is almost null around 5.5 GHz. This is also verified by individual parametric studies.

The simulated and measured far field radiation patterns of the proposed antenna at centre

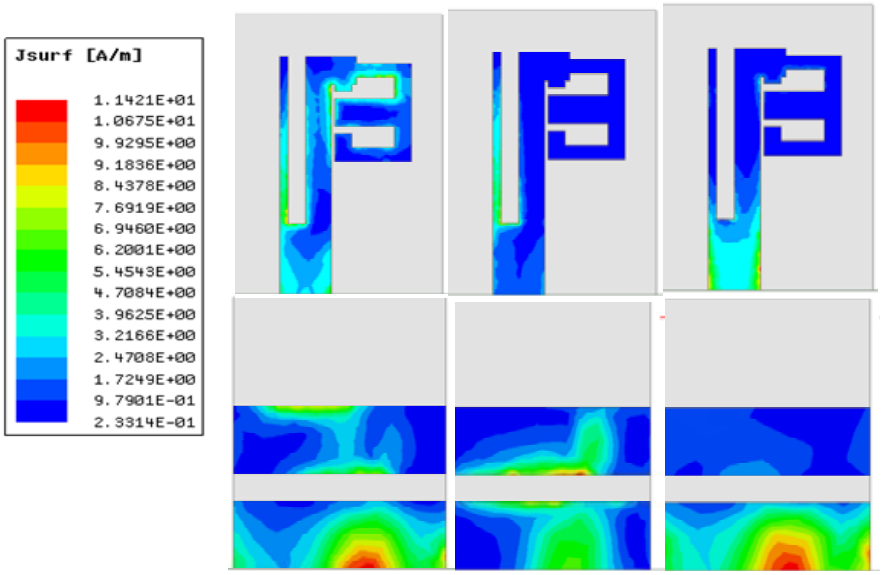

Figure 10. Simulated surface current distribution of the proposed antenna at (a) 2.4 GHz, (b) 3.5 GHz, (c) 5.5 GHz.

frequencies 2.4 GHz, 3.5 GHz, and 5.5 GHz are shown in Figs. 11(a), (b), and (c), respectively. It is observed that the radiation is nearly bidirectional in the E plane and almost omnidirectional in the H plane for all the operating frequency bands. The simulated gain and radiation efficiency of the proposed antenna with metamaterial slab show an increase in these values over the entire operating region compared with the one without metamaterial as shown in Fig. 11(d). The antenna efficiency varies over a range of (50–65)% without metamaterial and over (60–80)% with metamaterial. The realized gain varies over (1.5–2.7) dB without metamaterial and (2–3) dB with metamaterial over the entire operating range. Consistent radiation pattern makes the antenna a suitable candidate in many portable wireless devices.

4. STRUCTURE OF THE PROPOSED METAMATERIAL

A structure of the proposed metamaterial composed of a 5×3 array of polygonal split rings is shown in Fig. 12. The split rings are printed on a $20 \times 13 \times 1.6\,\text{mm}^3$ FR-4 substrate. A unit cell split ring arrangement is shown in Fig. 12(b). The dimensions of the split ring are parameterized and are as follows: $L_9 = 4\,\text{mm}$; $W_7 = 4\,\text{mm}$; $W_8 = 1.3\,\text{mm}$; $W_9 = 2.4\,\text{mm}$; $W_{10} = 0.15\,\text{mm}$; $W_{11} = 0.2\,\text{mm}$. The analysis of this metamaterial is done using the classic waveguide method [33], in which the proposed slab is placed inside a waveguide of suitable dimension with no air gaps in the walls of fixture. A uniform plane wave is then incident upon the slab inducing electromagnetic resonance. The transmission and reflection characteristics are measured from the other port of the waveguide. The simulated S parameters are shown in Fig. 13. As observed from the figure, a wide stopband is achieved from 7.5 to 9 GHz, which actually contributes to the reduction in the SAR. This metamaterial structure, when being placed above the proposed antenna, exhibits a slight frequency shift, and thus it is claimed to reduce the SAR only at the upper resonant frequency of 5 GHz. The retrieved S parameters are then used in the expressions below to find the refractive index (n), effective permeability (μ), and permittivity (ε) [34]

$$n = \frac{1}{kd}\cos^{-1}\left[\frac{1}{2S_{21}}(1 - S_{11}^2 + S_{21}^2)\right] \tag{2}$$

$$z = \sqrt{\frac{(1+S_{11})^2 - S_{21}^2}{(1-S_{11})^2 - S_{21}^2}} \tag{3}$$

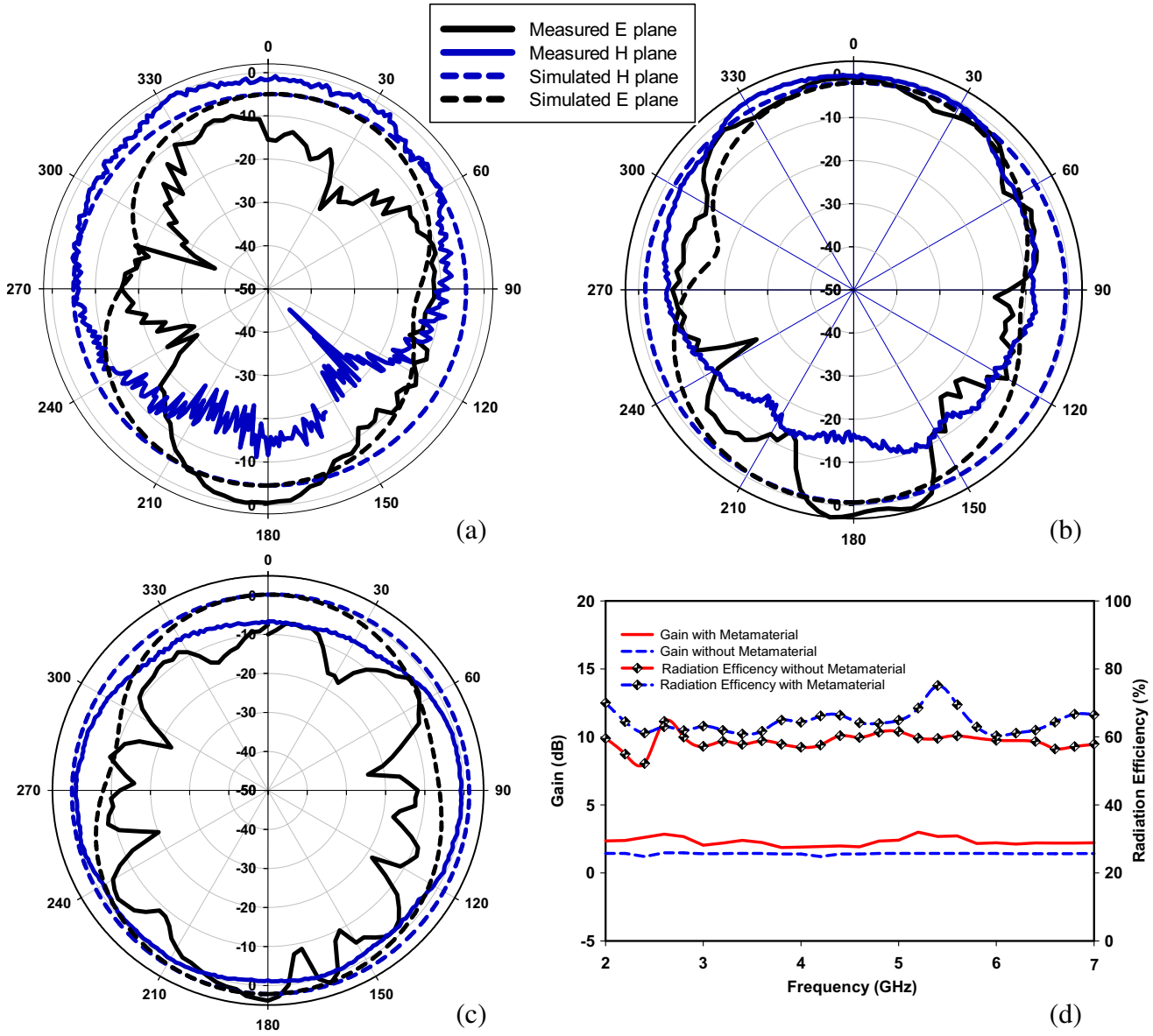

Figure 11. Simulated and measured E plane and H plane pattern of the proposed antenna at (a) 2.4 GHz, (b) 3.5 GHz and (c) 5 GHz [Measured — solid line, Simulated — Dashed line, E plane — Black, H plane — Blue], (d) simulated gain (dB) and radiation efficiency (%) with and without the proposed metamaterial.

z is the wave impedance.

Now, n and z can be related to ε and μ by the expression:

$$\varepsilon = n/z \text{ and } \mu = nz \tag{4}$$

As shown in Fig. 14, the proposed structure exhibits negative permeability at 5.2 GHz, which claims it to be a metamaterial, also contributing for SAR reduction at that frequency.

With the inclusion of the metamaterial slab above the antenna, the resonances are inferred from (2.38–2.48) GHz, (3.34–3.56) GHz and (4.32–7.0) GHz. It is inferred that the obtained results are close to the one obtained without the metamaterial structure.

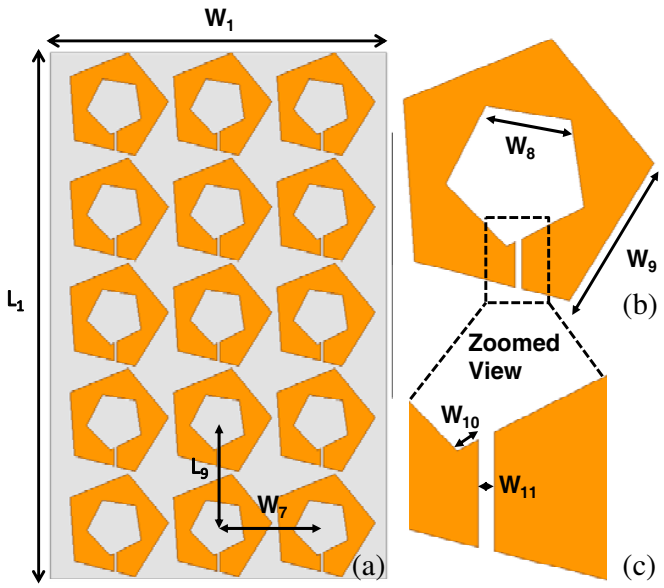

Figure 12. (a) Layout of the proposed metamaterial structure. (b) Unit cell split ring. (c) Photograph of the proposed antenna along with the metamaterial structure.

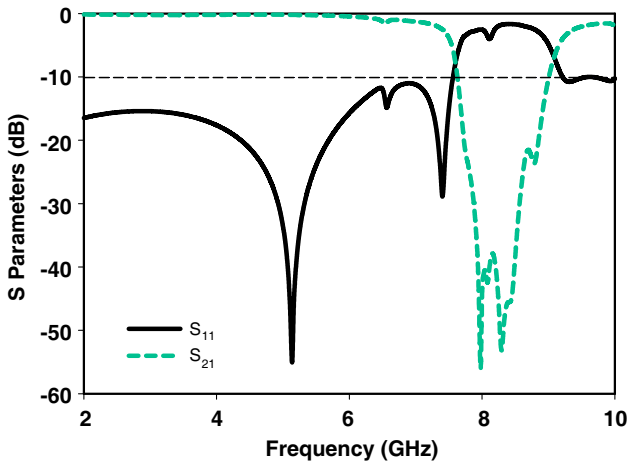

Figure 13. Simulated S parameters of the proposed metamaterial structure.

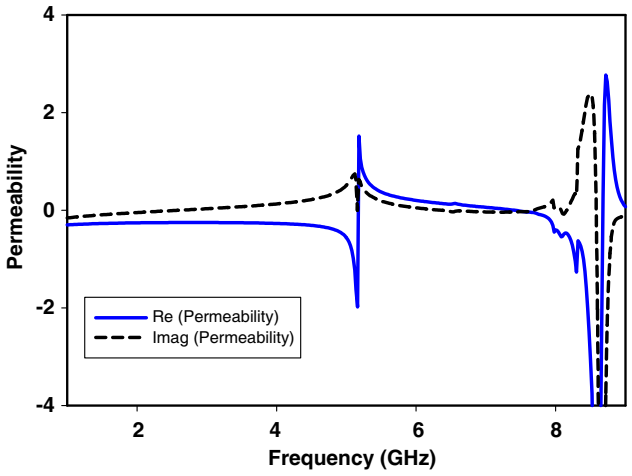

Figure 14. Extracted real and imaginary part of permeability of the proposed metamaterial.

5. EQUIVALENT CIRCUIT MODEL OF THE PROPOSED ANTENNA AND THE METAMATERIAL

The proposed split ring's resonant frequency is analyzed by the quasi-static equivalent circuit model [35]. The equivalent circuit model is shown in Fig. 16. The resonant frequency of a unit cell split ring resonators is given by,

$$\omega_0 = \frac{1}{\sqrt{L_s C_s}}$$

where L_s is the inductance of a single ring with the average radius of the resonator and the width of the rings being c. C_s can be obtained as,

$$L_s = \frac{\mu_0 A}{l}; \quad A = 5 * (W_9 - W_8) - W_{11}; \quad l = 2\pi a$$

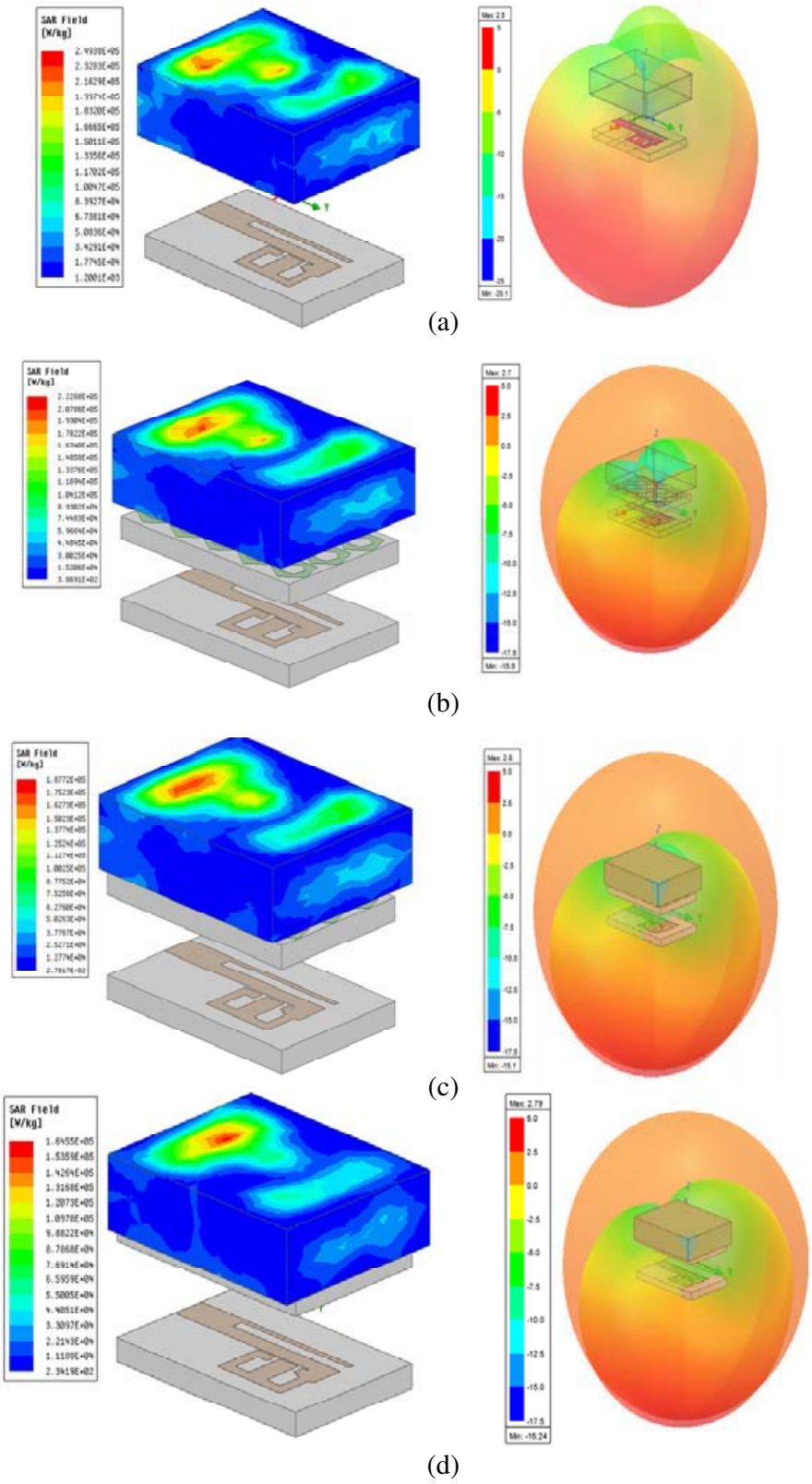

Figure 15. SAR values at different distance of the metamaterial structure from the antenna. (a) No metamaterial, (b) 6 mm, (c) 7 mm, (d) 8 mm.

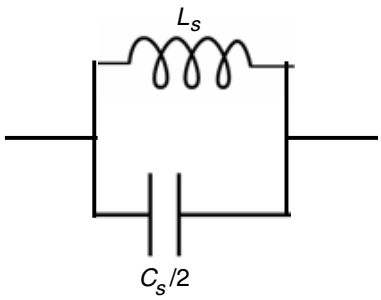

Figure 16. Equivalent circuit model of a unit cell split ring resonator.

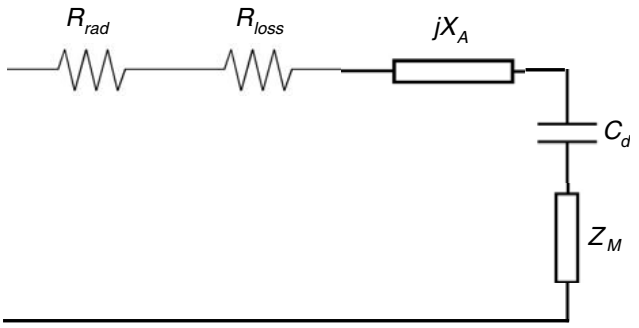

Figure 17. Equivalent circuit model of the proposed antenna along with the metamaterial slab.

$$C_s = 2\pi r C_{pul}$$

where C_{pul} represents the per unit length capacitance between the rings forming the resonator. Upon calculation, our unit cell split ring has $L_s = 1.63\,\mu\text{H}$ and $C_s = 0.01952\,\text{pF}$, yielding a resonant frequency of 5 approximately 5 GHz.

Figure 17 shows the equivalent circuit model of the proposed antenna along with the metamaterial slab. Here, R_{rad} denotes the radiation resistance, R_{loss} the loss resistance, X_A the antenna reactance, C_d the capacitance between the antenna and the metamaterial slab, and Z_M the metamaterial impedance.

6. SPECIFIC ABSORPTION RATE ANALYSIS

Specific Absorption Rate (SAR) is the measure of amount of power absorbed by 10 g or 1 g of tissue. Initially, a $20 \times 16 \times 5\,\text{mm}^3$ cubic tissue model is placed at a distance of 10 mm from the ground plane of the antenna. The chosen tissue model has the dielectric properties of a muscle with relative permittivity 46.7 and mass density $1.01\,\text{kg/m}^3$. The SAR is calculated in the HFSS environment with this setup and is found to be 2.49 W/kg. Later, the proposed metamaterial slab is placed in between the antenna and the muscle model. The distance between the antenna and the metamaterial slab is varied from 6 mm to 8 mm in steps of 1 mm, and the corresponding SAR values and radiation pattern displaying gain values are noted. This is shown in Figs. 15(a)–(d). It is inferred from the figure that the major part of the radiation is directed towards the ground plane as the distance between the metamaterial and antenna increases, which has contributed to the increase in gain as well as decrease in the SAR value.

Table 2 lists the $\text{SAR}_{1\,\text{g}}$ (W/Kg) value, corresponding decrease in SAR for several distances of the metamaterial slab from the proposed antenna, and the gain at several distances. The simulated gain of the antenna without the proposed metamaterial structure is observed as 2.7 dB, and with the structure at a distance of 8 mm, it is observed as 3.0 dB contributing to 30% increase in the antenna gain. Table 3 lists the comparison of the proposed metamaterial's SAR reduction percentage and gain with the other structures that are discussed in the recent literature. It is inferred that the proposed structure for SAR reduction is compact in size compared with the others proposed in [26–32]. However, the multi split

Table 2. $\text{SAR}_{1\,\text{g}}$ values at different distance from the antenna.

$\text{SAR}_{1\,\text{g}}$ value without metamaterial		**2.49 W/kg**	
Distance of Metamaterial from the Antenna (mm)	$\text{SAR}_{1\,\text{g}}$ Value (W/kg)	Percentage Reduction in SAR	Gain (dB)
6	2.268	22.2	2.7
7	1.877	61.3	2.8
8	1.645	84.5	3.0

Table 3. Comparison of the proposed antenna with the previous literature.

Reference antenna	Metamaterials used	Size of the proposed structure	Gain (dBi)	Tissue Model Used	Maximum Percentage Reduction in SAR
[15]	Array of square SRRs	$45 \times 45 \times 6$	Not Specified	Cubical Tissue Model	37.62
[16]	Single Rectangular SRR	$35 \times 34 \times 0.8\,\text{mm}^3$	3.11	Cubical Tissue Model	13.30
[17]	Single Circular SRR	$24.8 \times 24.8 \times 0.8$	Not Specified	Spherical Layered Tissue Model	93.00
[18]	Meta surface	$72 \times 72 \times 1$	2.88	Human Phantom Model	101.00
[19]	Embroidered SRRs	$85 \times 70 \times 3.2$	7.81	Human Head Model	94.00
[20]	Metallic casing loop	$140 \times 74.6 \times 3.2$	1.25	Human Head Model	18.00
[21]	Multi split square ring metamaterial	$11 \times 11 \times 1.6$	Not Specified	Human Head Model	45.54
This work	Polygonal split rings	$20 \times 13 \times 1.6$	3	Cubical Tissue Model/ Human Head Model	84.50/55.72

square ring metamaterial in [32] is more compact, and yet the percentage reduction achieved in the proposed work is more than that of the former. However, the tissue models considered in both the cases are different, and therefore the comparison might not be fair.

7. CONCLUSION

A slotted antenna with conjoint split rings is presented in this paper. The antenna operates in the WLAN (2.4 GHz and 5.5 GHz) and WiMAX (3.5 GHz) bands. A metamaterial slab of same dimension as that of the antenna is placed at a suitable distance from the antenna to yield SAR reduction. The metamaterial increases the gain of the antenna and tends to reduce the SAR of the tissue. The maximum SAR reduction achieved is 84.5% with a 30% increase in gain of the antenna. The radiation pattern and gain of the antenna are found satisfactory making it suitable for wireless communication devices.

DECLARATION OF INTEREST

The authors report no conflicts of interest.

REFERENCES

1. Gautam, A. K., A. Bisht, and B. K. Kanaujia, "A wideband antenna with defected ground plane for WLAN/WiMAX applications," *AEU-International Journal of Electronics and Communications*, Vol. 70, No. 3, 354–358, 2016.
2. Saraswat, R. K. and M. Kumar, "Miniaturized slotted ground UWB antenna loaded with metamaterial for WLAN and WiMAX applications," *Progress In Electromagnetics Research*, Vol. 65, 65–80, 2016.
3. Li, L., et al., "A compact triple-band printed monopole antenna for WLAN/WiMAX applications," *IEEE Antennas and Wireless Propagation Letters*, Vol. 15, 1853–1855, 2016.
4. Hoang, T. V., et al., "Quad-band circularly polarized antenna for 2.4/5.3/5.8-GHz WLAN and 3.5-GHz WiMAX applications," *IEEE Antennas and Wireless Propagation Letters*, Vol. 15, 1032–1035, 2015.
5. Naidu, P. V., A. Malhotra, and R. Kumar, "A compact ACS-fed dual-band monopole antenna for LTE, WLAN/WiMAX and public safety applications," *Microsystem Technologies*, Vol. 22, No. 5, 1021–1028, 2016.

6. Mathew, S., et al., "Compact dual polarised V slit, stub and slot embedded circular patch antenna for UMTS/WiMAX/WLAN applications," *Electronics Letters*, Vol. 52, No. 17, 1425–1426, 2016.
7. Kunwar, A., A. K. Gautam, and B. K. Kanaujia, "Inverted L-slot triple-band antenna with defected ground structure for WLAN and WiMAX applications," *International Journal of Microwave and Wireless Technologies*, Vol. 9, No. 1, 191–196, 2017.
8. Ahmad, H., et al., "Compact triband slotted printed monopole antenna for WLAN and WiMAX applications," *International Journal of RF and Microwave Computer-Aided Engineering*, 2019.
9. Nelaturi, S. and N. V. S. N. Sarma, "A compact microstrip patch antenna based on metamaterials for Wi-Fi and WiMAX applications," *Journal of Electromagnetic Engineering and Science*, Vol. 18, No. 3, 182–187, 2018.
10. Ali, T., et al., "A multiband antenna loaded with metamaterial and slots for GPS/WLAN/WiMAX applications," *Microwave and Optical Technology Letters*, Vol. 60, No. 1, 79–85, 2018.
11. Li, H., et al., "Dual-band planar antenna loaded with CRLH unit cell for WLAN/WiMAX application," *IET Microwaves, Antennas & Propagation*, Vol. 12, No. 1, 132–136, 2017.
12. Alibakhshikenari, M., et al., "A comprehensive survey of "Metamaterial transmission-line based antennas: Design, challenges, and applications"," *IEEE Access*, Vol. 8, 144778–144808, 2020.
13. Alibakhshikenari, M., et al., "Super-wide impedance bandwidth planar antenna for microwave and millimeter-wave applications," *Sensors*, Vol. 19, No. 10, 2306, 2019.
14. Alibakhshi-Kenari, M., M. Naser-Moghadasi, and R. A. Sadeghzadeh, "Bandwidth and radiation specifications enhancement of monopole antennas loaded with split ring resonators," *IET Microwaves, Antennas & Propagation*, Vol. 9, No. 14, 1487–1496, 2015.
15. Alibakhshi-Kenari, M., M. Naser-Moghadasi, and R. Sadeghzadeh, "The resonating MTM-based miniaturized antennas for wide-band RF-microwave systems," *Microwave and Optical Technology Letters*, Vol. 57, No. 10, 2339–2344, 2015.
16. Alibakhshi-Kenari, M., et al., "Miniature CRLH-based ultra wideband antenna with gain enhancement for wireless communication applications," *ICT Express*, Vol. 2, No. 2, 75–79, 2016.
17. Alibakhshikenari, M., et al., "Miniaturised planar-patch antenna based on metamaterial L-shaped unit-cells for broadband portable microwave devices and multiband wireless communication systems," *IET Microwaves, Antennas & Propagation*, Vol. 12, No. 7, 1080–1086, 2018.
18. Alibakhshikenari, M., B. S. Virdee, and E. Limiti, "Compact single-layer traveling-wave antenna design using metamaterial transmission lines," *Radio Science*, Vol. 52, No. 12, 1510–1521, 2017.
19. Alibakhshi-Kenari, M., et al., "New CRLH-based planar slotted antennas with helical inductors for wireless communication systems, RF-circuits and microwave devices at UHF-SHF bands," *Wireless Personal Communications*, Vol. 92, No. 3, 1029–1038, 2017.
20. Alibakhshi-Kenari, M., et al., "Periodic array of complementary artificial magnetic conductor metamaterials-based multiband antennas for broadband wireless transceivers," *IET Microwaves, Antennas & Propagation*, Vol. 10, No. 15, 1682–1691, 2016.
21. Alibakhshi-Kenari, M., et al., "New compact antenna based on simplified CRLH-TL for UWB wireless communication systems," *International Journal of RF and Microwave Computer-Aided Engineering*, Vol. 26, No. 3, 217–225, 2016.
22. Alibakhshi-Kenari, M., et al., "Metamaterial-based antennas for integration in UWB transceivers and portable microwave handsets," *International Journal of RF and Microwave Computer-Aided Engineering*, Vol. 26, No. 1, 88–96, 2016.
23. Sallam, M. O., et al., "Wideband CPW-fed flexible bow-tie slot antenna for WLAN/WiMax systems," *IEEE Transactions on Antennas and Propagation*, Vol. 65, No. 8, 4274–4277, 2017.
24. Priyadarshini, S. J. and D. J. Hemanth, "Investigation and reduction methods of specific absorption rate for biomedical applications: A survey," *International Journal of RF and Microwave Computer-Aided Engineering*, Vol. 28, No. 3, e21211, 2018.
25. Stephen, J. P. and D. J. Hemanth, "An investigation on specific absorption rate reduction materials with human tissue cube for biomedical applications," *International Journal of RF and Microwave Computer-Aided Engineering*, e21960, 2019.

26. Hwang, J.-N. and F.-C. Chen, "Reduction of the peak SAR in the human head with metamaterials," *IEEE Transactions on Antennas and Propagation*, Vol. 54, No. 12, 3763–3770, 2006.
27. Saraswat, R. K. and M. Kumar, "A metamaterial hepta-band antenna for wireless applications with specific absorption rate reduction," *International Journal of RF and Microwave Computer-Aided Engineering*, Vol. 29, No. 10, e21824, 2019.
28. Imaculate Rosaline, S. and S. Raghavan, "Design and analysis of a SRR superstrate for SAR reduction," *Journal of Electromagnetic Waves and Applications*, Vol. 29, No. 17, 2330–2338, 2015.
29. Janapala, D. K., et al., "Specific absorption rate reduction using metasurface unit cell for flexible polydimethylsiloxane antenna for 2.4 GHz wearable applications," *International Journal of RF and Microwave Computer-Aided Engineering*, Vol. 29, No. 9, e21835, 2019.
30. Gil, I., R. Seager, and R. Fernández-García, "Embroidered metamaterial antenna for optimized performance on wearable applications," *Physica Status Solidi (A)*, Vol. 215, No. 21, 1800377, 2018.
31. Nazeri, A., A. Abdolali, and M. Mehdi, "An extremely safe low-SAR antenna with study of its electromagnetic biological effects on human head," *Wireless Personal Communications*, 1–14, 2019.
32. Ramachandran, T., et al., "Specific absorption rate reduction of multi split square ring metamaterial for L- and S-band application," *Results in Physics*, 102668, 2019.
33. Chen, H., J. Zhang, Y. Bai, et al., "Experimental retrieval of the effective parameters of metamaterials based on a waveguide method," *Opt. Express.*, Vol. 14, 12944–12949, 2006, 10.1364/OE.14.012944.
34. Smith, D. R., et al., "Electromagnetic parameter retrieval from inhomogeneous metamaterials," *Physical Review E*, Vol. 71, No. 3, 036617, 2005.
35. Baena, J. D., J. Bonache, F. Martín, R. Marques, F. Falcone, T. Lopetegi, M. Laso, J. García-García, I. Gil, M. Portillo, and M. Sorolla Ayza, "Equivalent-Circuit models for split-ring resonators and complementary split-ring resonators coupled to planar transmission lines," *IEEE Transactions on Microwave Theory and Techniques*, Vol. 53, 1451–1461, 2005, 10.1109/TMTT.2005.845211.